

The Role of the Apical Oxygen in Cuprate High-Temperature Superconductors

Samuel Vadnais,^{1,2, a} Rémi Duchesne,² Kristjan Haule,³ A.-M. S. Tremblay,² David Sénéchal,² and Benjamin Bacq-Labreuil^{4,2, b}

¹*Department of Physics, University of Toronto, Toronto, Ontario, Canada, M5S 1A1*

²*Département de physique, Regroupement québécois sur les matériaux de pointe & Institut quantique Université de Sherbrooke, 2500 Boul. Université, Sherbrooke, Québec J1K2R1, Canada*

³*Center for Materials Theory, Department of Physics & Astronomy, Rutgers University, Piscataway, New Jersey 08854, USA*

⁴*Université de Strasbourg, CNRS, Institut de Physique et Chimie des Matériaux de Strasbourg, UMR 7504, F-67000 Strasbourg, France*

(Dated: January 23, 2026)

Scanning tunneling microscopy measurements exploiting the natural superstructure modulation of the cuprate superconductor $\text{Bi}_2\text{Sr}_2\text{CaCu}_2\text{O}_{8+x}$ (Bi-2212) have revealed a possible correlation between the Cu-apical-O distance δ_{api} and the superconducting order parameter m_{SC} , as reported recently by O’Mahony *et al.* (Proc. Natl. Acad. Sci. 119, e2207449119 (2022)). These observations were interpreted as evidence for a direct link between superconductivity and the charge-transfer gap, and more broadly revived the long-standing question of the role of apical oxygens in cuprate superconductivity. Using a combination of density-functional theory and cluster dynamical mean-field theory, we compute from first principles the variations of m_{SC} induced solely by apical oxygen displacement in $\text{Bi}_2\text{Sr}_2\text{CuO}_{6+\delta}$, Bi-2212, and $\text{HgBa}_2\text{CuO}_{4+\delta}$. The quantitative agreement between our calculations and experiments allows us to unambiguously attribute the observed variations of m_{SC} to changes in δ_{api} . We demonstrate, however, that these variations of m_{SC} originate predominantly from changes in the effective hole-doping of the CuO_2 planes, with negligible effect on the charge-transfer gap. The modest magnitude of the m_{SC} modulation induced by apical-oxygen displacement alone therefore warrants caution in interpreting correlations between T_c and δ_{api} inferred from comparisons across different cuprate compounds.

Introduction Considerable progress has been made in identifying physical parameters that optimize the superconducting transition temperature (T_c) of cuprate superconductors. In particular, several experimental correlations have been found between increasing T_c and (i) maximizing oxygen hole content [1–5], (ii) stronger superexchange interaction [6], and (iii) reduced charge transfer gap [7, 8]. These correlations have been reproduced simultaneously in model calculations [9]. At the same time, advances in first-principles-based approaches [10–12] raise the prospect that the long-standing problem of high- T_c superconductivity in cuprates may be addressed quantitatively.

Despite this progress, important questions remain unresolved, including the long-standing issue of the relationship between the apical oxygen distance (δ_{api}) and the superconductivity in cuprates [10, 13–19].

Here, we revisit this problem motivated by an unexpected experimental observation. A striking scanning tunnelling microscopy (STM) study of optimally-doped $\text{Bi}_2\text{Sr}_2\text{CaCu}_2\text{O}_{8+x}$ (Bi-2212) revealed a strong correlation between the well-known super-structure modulation and the density of Cooper pairs, proportional to the squared superconducting order parameter $|m_{\text{SC}}|^2$ [20]. The authors proposed that the super-structure modulation can be primarily understood as a modulation of δ_{api} , which in turn induces a spatial variation in the charge-transfer gap (CTG). This interpretation relies on the assumption that increasing δ_{api} reduces the CTG [20] and thereby enhances m_{SC} [8, 10].

Numerous studies have proposed correlations between the apical oxygen distance δ_{api} and T_c by comparing different cuprate families [10, 14, 15, 18]. These approaches implicitly assume that complex chemical and structural differences

across materials can be effectively reduced to variations of a single parameter, δ_{api} , leaving unresolved the question of whether there exists a direct causal link with T_c . A few works attempted to isolate the specific role of δ_{api} . Feiner *et al.* studied the coupling to out-of-plane degrees of freedom within a five-band Hubbard model [13], focusing in particular on how apical oxygen hybridization affects the contribution of Cu- d_{z^2} -like orbitals to the low-energy Zhang-Rice (ZR) [21] band. This line of reasoning connects naturally to more recent studies which, without explicitly considering the apical oxygen, argue that pushing the Cu- d_{z^2} orbital away from the Fermi level is favorable for superconductivity [22, 23]. The isolated effect of apical oxygen on the parameters of low-energy effective models for cuprates has also been studied in Refs. 16 and 17. Nevertheless, as in Ref. 13, a direct impact on the superconducting properties could not be established. Finally, a more recent study by Acharya *et al.* employed advanced *ab initio* methods to relate controlled displacements of the apical oxygen in La-based cuprates to changes in m_{SC} [19]. However, m_{SC} was assessed without explicitly considering hole-doping; strong correlations were treated at the level of single-site DMFT; and superconductivity was inferred using a Bardeen–Cooper–Schrieffer-based ansatz, whose applicability to cuprates is questionable.

Here, we address three crucial questions that have remained unanswered to date: (i) Can the effect of apical oxygen displacements on the superconducting properties of cuprates be quantified? (ii) Are the apical oxygen displacements alone sufficient to account for the experimentally observed periodic variations of m_{SC} in Bi-based cuprates? (iii) Does the charge-transfer gap mediate the relationship between δ_{api} and m_{SC} ?

We answer these three questions using a recently developed

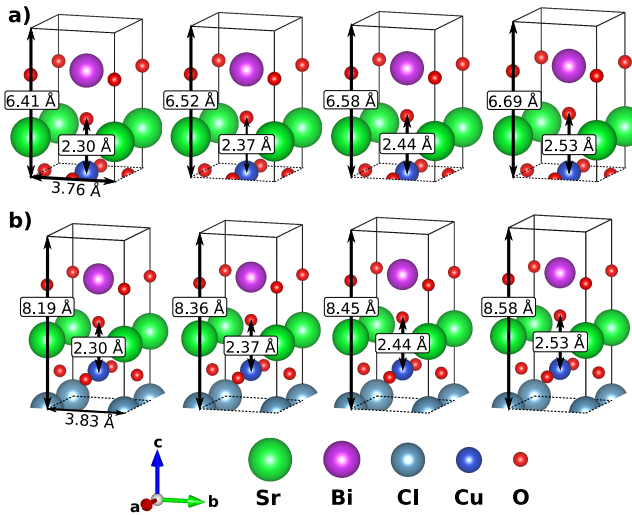


FIG. 1. Half simplified ($P4/mmm$) unit cells of (a) Bi-2201 and (b) Bi-2212. δ_{api} , $c/2$ and a are displayed (See SM [30] for details).

ab initio framework [12] that enables first-principles predictions of the superconducting order parameter m_{SC} by combining density functional theory (DFT) [24, 25] with cluster dynamical mean-field theory (CDMFT) [26–29]. By performing calculations on single-layer $\text{Bi}_2\text{Sr}_2\text{CuO}_{6+\delta}$ (Bi-2201) and bi-layer Bi-2212 in which only δ_{api} is varied, we quantitatively reproduce the experimental observations of O’Mahony *et al.* [20]. Our approach enables us to assign an absolute scale to the experimentally measured relative variations of $|m_{\text{SC}}|^2$, and to show that the effect of δ_{api} is small compared to other changes in the crystal structure. This implies that the proposed correlation between δ_{api} and T_c inferred from comparisons across different cuprate families [10, 14, 15, 18] should be treated with caution. Finally, our calculations reveal that variations of m_{SC} with δ_{api} cannot be explained by changes in the CTG. Instead, we find that apical oxygen displacements primarily act by modulating the *effective* hole doping of the CuO_2 planes, involving the $\text{Cu-}d_{x^2-y^2}$ and $\text{O-}p_{x/y}$ orbitals, which in turn controls m_{SC} . We perform additional calculations for $\text{HgBa}_2\text{CuO}_{4+\delta}$ (Hg-1201), which further support this interpretation. Our work establishes that variations in the *effective* hole doping of the CuO_2 planes play a central role and must be carefully accounted for.

Method A fully first-principles description of m_{SC} in Bi-2201 and Bi-2212 that explicitly incorporates the long-range superstructure modulation is currently intractable. STM measurements show that this modulation produces stripe-like regions, in which the tetragonal crystal structure is preserved, along the diagonals of the CuO_2 planes with respect to the a and b axes [20, 31, 32]. The short superconducting coherence length in cuprates [33], together with the success of previous small cluster DMFT calculations for superconductivity, suggests that the dominant contribution arises from local structural variations of δ_{api} . Accordingly, we perform calculations

for homogeneous Bi-2201/2212 structures with four distinct values of δ_{api} , chosen to match the distances observed experimentally [20], as illustrated in Fig. 1 [34].

Since atomic displacements involve energy scales much larger than those related to superconductivity, we optimized the Bi-2201 unit cell parameters (a , c) and internal atomic positions using the eDMFT approach [35–37], while keeping the apical oxygen distance δ_{api} fixed. Increasing δ_{api} leads to an expansion of the c lattice parameter, while a remains essentially unchanged. The Bi-2212 structures were constructed empirically by assuming that the dependence of a and c on δ_{api} follows the same trends as in Bi-2201. The resulting cell parameters a , c , and δ_{api} are summarized in Fig. 1.

We then compute m_{SC} in Bi-2201 and Bi-2212 using the DFT+CDMFT framework of Ref. 12. We construct 2×2 supercells, with a correlated subspace restricted to four $\text{Cu-}d_{x^2-y^2}$ orbitals, and perform DFT+CDMFT calculations at effectively zero temperature with $U = 9$ eV. Since Bi-2201 and Bi-2212 are naturally self-doped [38, 39], no virtual crystal approximation (VCA) [40] is required. These calculations employ the eDMFT package [12, 35–37], extending Wien2k [41] to DFT with (C)DMFT, and combined with the exact diagonalization solver implemented in PyQCM [42]. The Wannier90 package [43, 44] is used to construct maximally localized Wannier orbitals used in Fig. 3 and End Matter (EM). We refer to the SM for more computational details [30] and to Ref. 12 for an in-depth presentation of our DFT+CDMFT framework.

Results We first address the above questions (i) and (ii) by showing how m_{SC} varies with δ_{api} in Bi-based cuprates. We then answer (iii) in two steps. By downfolding to an effective three-band model, we demonstrate that the CTG *increases* with increasing δ_{api} , thereby ruling out the scenario of Ref. 20. This result leads to our central conclusion: the variation of the SC order parameter is instead governed by the change in effective doping induced by the apical oxygen displacement. Finally, we substantiate this conclusion by extending our analysis to Hg-1201.

Figure 2 presents the computed m_{SC} in Bi-2201/2212. The absolute variation of m_{SC} with δ_{api} is relatively weak, of order 0.5×10^{-2} for both compounds, and approximately three times smaller than the difference between m_{SC} for Bi-2201 and Bi-2212. Note that m_{SC} of Bi-2201 is about twice that of Bi-2212, consistent with the measured T_c of Bi-2212 being nearly twice that of Bi-2201 [6, 8].

The relative variations of the superfluid density, $|m_{\text{SC}}|^2/|m_{\text{SC}}|^2$, show remarkable quantitative agreement with the STM measurements reported in Ref. 20 on Bi-2212 (see Fig. 2). The computed variations in Bi-2212 exhibit a slightly more pronounced curvature. We attribute this to the construction of the unit cells, in which the same c -axis versus δ_{api} relation as in Bi-2201 was assumed. This modeling choice does not affect our central conclusion: the apical oxygen displacement alone accounts for the measured variations of $|m_{\text{SC}}|^2$ associated with superstructure modulations in Bi-2212, and is expected to apply similarly to

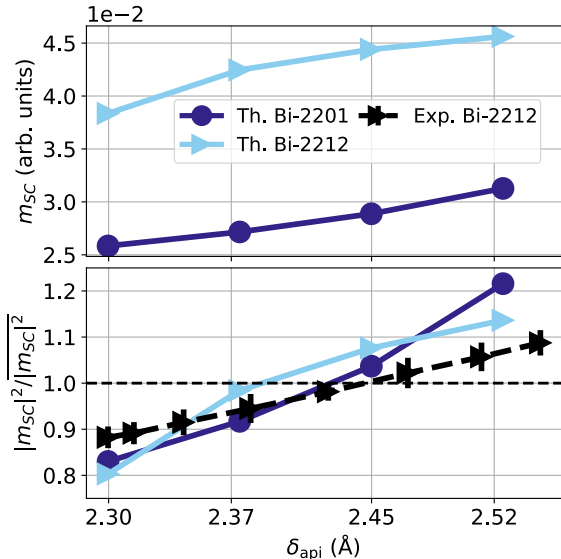


FIG. 2. Computed superconducting order parameter m_{SC} vs δ_{api} for Bi-2201 and Bi-2212 (top). Note the scaling of the y axis. Relative variations of the computed and measured superfluid density $|m_{\text{SC}}|^2 / |m_{\text{SC}}|^2$ vs δ_{api} (bottom). The experimental data are digitized from Ref. 20.

Bi-2201 [8]. Our analysis further shows that these variations are small compared to the differences observed between different cuprate materials. This observation calls for caution when interpreting the proposed correlation between δ_{api} and T_c [10, 14, 15, 18].

Before examining whether the CTG could be the link between m_{SC} and δ_{api} , we first clarify its definition. The CTG corresponds to the energy required to transfer an electron from an O to a Cu atom. In *undoped* cuprates, the CTG coincides with the spectral gap because (i) the highest occupied O- p states belong to the low-energy ZR band, and (ii) the lowest unoccupied Cu- d states form the upper Hubbard band [12]. Upon hole-doping, strong electronic correlations are known to induce substantial spectral weight transfer of Cu- d character to energies just above the Fermi level [12, 45]. A strict application of the above definition, therefore, implies that the CTG vanishes in hole-doped *metallic* compounds. To address this issue, theoretical studies have introduced modified definitions of the CTG, such as the energy separation between the upper edge of the ZR singlet (above the Fermi level) and the upper Hubbard band [9], or the difference between the on-site energies of the Cu- $d_{x^2-y^2}$ and O- $p_{x/y}$ orbitals [10]. All of these definitions associate variations of the CTG in hole-doped compounds with changes in the electronic structure *above* the Fermi level, which itself remains fixed. Crucially, none of these definitions corresponds to that employed in Ref. 20, where the proposed CTG variations are instead inferred from a redistribution of spectral weight *below* the Fermi level based on an arbitrary threshold.

To avoid ambiguity, we examine the variations of the CTG with respect to δ_{api} in the undoped systems. To eliminate

the self-doping intrinsic to Bi-based cuprates, we consider an effective Emery–Varma–Schmitt–Rink–Abrahams model [46, 47]. Setting the Cu- $d_{x^2-y^2}$ on-site energy to zero, Δ_p denotes the on-site energy of the O- $p_{x/y}$ orbitals, μ is the chemical potential, and t_{pd} (t_{pp}) are the Cu–O (nearest O–O) hopping amplitudes (see SM [30]). For each value of δ_{api} , these parameters are obtained by constructing maximally localized Wannier orbitals from a DFT-only calculation for Bi-2201. The energy separation between Cu and O orbitals requires a double-counting correction, for which we adopt the nominal scheme [35, 48, 49]. Assuming one electron per Cu- $d_{x^2-y^2}$ orbital, Δ_p is then given by $\Delta_p = \epsilon_p^{\text{DFT}} - \epsilon_d^{\text{DFT}} + \frac{U}{2}$, where $\epsilon_{p(d)}^{\text{DFT}}$ are the on-site energies of the Wannier orbitals.

We show in Fig. 3(a,b) t_{pd} , t_{pp} and $(\epsilon_p^{\text{DFT}} - \epsilon_d^{\text{DFT}})$ with respect to δ_{api} . The hopping parameters remain essentially constant. By contrast, $(\epsilon_p^{\text{DFT}} - \epsilon_d^{\text{DFT}})$ decreases by a small but significant amount of approximately $\sim 3 - 4\%$, while δ_{api} varies by about 10%. From a simplified mean-field perspective, the bare CTG is expected to scale as $\Delta_{\text{CTG}} \simeq U - \Delta_p$. Since the hopping amplitudes are nearly constant and Δ_p decreases with increasing δ_{api} , Δ_{CTG} is therefore expected to be an *increasing* function of δ_{api} , in direct contradiction with the interpretation of Ref. 20.

To complete this argument, it is necessary to examine the δ_{api} dependence of the on-site interaction U on the Cu- $d_{x^2-y^2}$ orbitals. We estimated U using constrained DFT [50] with $\sqrt{5} \times \sqrt{5}$ supercells. Although this approach is known to underestimate U for cuprates, and the supercells we consider are modest, this does not affect our conclusion since we focus exclusively on relative variations. As shown in Fig. 3(c), U is found to be a *slowly increasing* function of δ_{api} , reflecting the reduced screening on the Cu- d orbitals as the apical oxygen moves away from the Cu site. Accounting for the δ_{api} dependence of U therefore further reinforces our conclusion that the CTG is an increasing function of δ_{api} .

To further substantiate our interpretation, we compute the superexchange interaction J of the 3-band model using a more appropriate $U = 9$ eV (same as in the DFT+CDMFT calculations) and exact diagonalization of Cu_2O_{25} clusters [51]. The energy difference between the lowest-energy singlet and triplet states provides an estimate of J . The resulting values are close to the experimentally reported estimates (~ 150 meV [6, 18]) and most importantly, J is found to be a decreasing function of δ_{api} (see Fig. 3). Since $J \propto t_{\text{eff}}^2 / \text{CTG}$, the observed decrease of J is internally consistent. A decreasing J is incompatible with the increase of m_{SC} [6], and therefore the CTG scenario proposed in Ref. 20 is not viable.

Although our analysis focuses on Bi-2201 for convenience, the conclusions directly extend to Bi-2212. Additional confirmation is provided in the SM [30] by a direct DFT+CDMFT evaluation of the CTG in insulating Hg-1201.

Our analysis calls for a new interpretation of the dI/dV measurements of Ref. 20 (see Fig. 3B therein). As discussed above, variations of the CTG in hole-doped cuprates should manifest as changes in the *unoccupied* part of the electronic

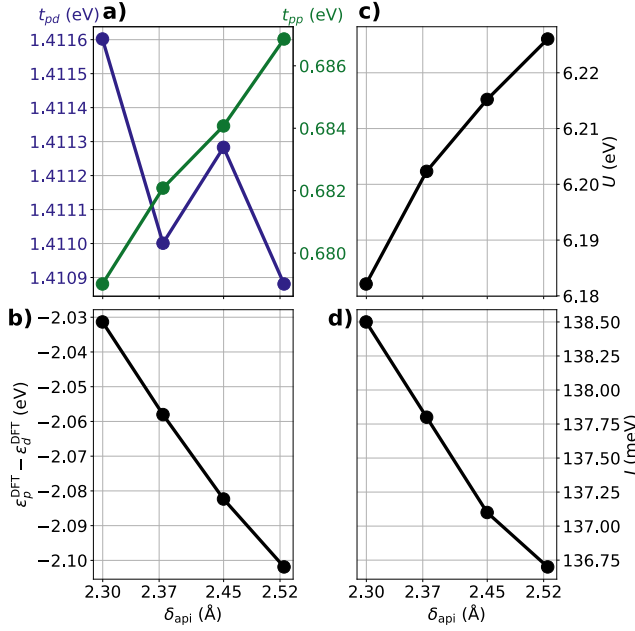


FIG. 3. (a) t_{pd} and t_{pp} (Wannier), (b) $(\varepsilon_p^{DFT} - \varepsilon_d^{DFT})$ (Wannier), (c) U (constrained DFT) and (d) J (Cu_2O_{25} clusters) vs δ_{api} . All parameters were computed for Bi-2201.

spectrum. Instead, the dI/dV measurements reveal variations of the spectral weight predominantly in the *occupied* part of the spectrum [20], consistent with changes in the effective occupation of the CuO_2 planes.

We therefore analyze the electron occupation of the CuO_2 planes obtained from our *ab-initio* DFT+CDMFT calculations for Bi-2201 and Bi-2212. We consider the variation of the occupation of the $\text{Cu-}d_{x^2-y^2}$ and $\text{O-}p_{x/y}$ orbitals, Δn_{CuO_2} , around the value obtained for the minimal δ_{api} , as shown in Fig. 4(a). In both Bi-2201 and Bi-2212, we observe an increase in electron occupation, corresponding to a reduction of the effective hole doping with increasing δ_{api} . Because self-doping places the CuO_2 planes in the overdoped regime (see EM), increasing δ_{api} drives the CuO_2 planes closer to optimal doping. This, in turn, leads to an enhancement of m_{SC} (see Fig. 4(b,c)) reflecting its strong sensitivity to doping. Quantitatively, variations of δ_{api} by $\sim 10\%$ induces changes in the effective doping of about $\sim 5\%$ ($\sim 2\%$ per CuO_2 plane) in Bi-2201 (Bi-2212). Despite the weaker per-plane doping variations in the bi-layer compound, the relative changes in m_{SC} are comparable to those observed in single-layer Bi-2201.

The same analysis is repeated for Hg-1201, for which calculations can be carried out in the underdoped regime. We fix a total doping of 15% using VCA [40], corresponding to an effective doping of approximately $\sim 11 - 12\%$ in the CuO_2 planes [12]. Hg-1201 structures were constructed in a similar way to Bi-2212, except that the apical oxygen distances are systematically larger in Hg-1201 (see SM [30]): $\delta_{\text{api}}^{\text{Hg}} \in [2.56, 2.81] \text{ \AA}$, $\delta_{\text{api}}^{\text{Bi}} \in [2.3, 2.52] \text{ \AA}$. Remarkably, Δn_{CuO_2} is found to anti-correlate with δ_{api} . Since Hg-1201

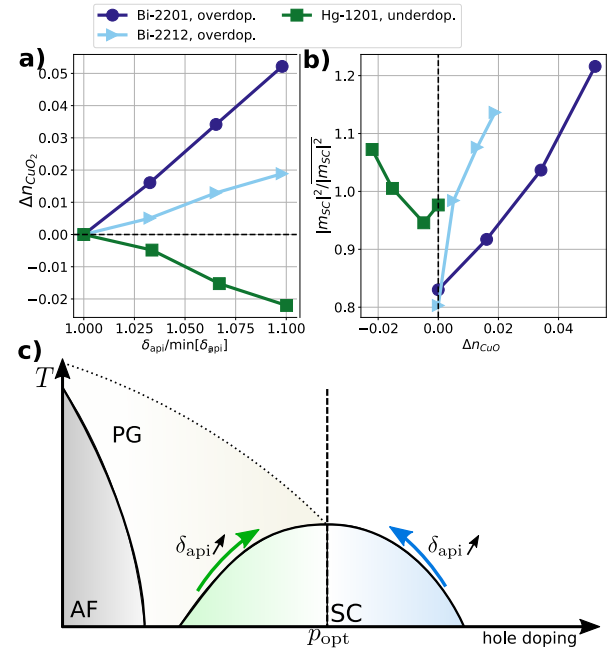


FIG. 4. (a) Electron occupation variations Δn_{CuO_2} of the in-plane $\text{Cu-}d_{x^2-y^2}$ and $\text{O-}p_x/p_y$ orbitals vs $\delta_{\text{api}}/\min[\delta_{\text{api}}]$. (b) Relative variations of the superfluid density $|m_{\text{SC}}|^2/|m_{\text{SC}}0|^2$ vs Δn_{CuO_2} . (c) Representative sketch of the cuprates phase diagram. m_{SC} is an increasing function of δ_{api} in all compounds since the effective hole doping increases in underdoped Hg-1201 (green), while it decreases in overdoped Bi-2201 and Bi-2212 (blue).

is here underdoped, we find that m_{SC} again increases with increasing δ_{api} , as shown in Fig. 4(a,b). These results are schematically summarized in Fig. 4(c). A detailed analysis of the δ_{api} dependence of m_{SC} in Hg-1201 is provided in SM [30].

It is remarkable that increasing δ_{api} leads to opposite trends in Δn_{CuO_2} in Hg-1201, compared to Bi-2201/2212. It deserves analysis. We find it fruitful to think of the charge transfer processes in terms of distinct *channels*. All compounds considered here share a first common channel: achieving the favorable oxidation state of all atoms requires the charge reservoir layers to donate electrons to the CuO_2 planes globally. It is reasonable to expect that increasing δ_{api} similarly weakens this channel in *all compounds* because it has the same physical origin, thereby leading to *increased* effective hole-doping, as in Hg-1201. For Bi-2201/2212, however, a second channel is present, associated with the Bi-O self-doping bands, which promote charge transfer in the opposite direction – from the CuO_2 planes to the charge reservoirs. Weakening this channel, therefore, results in a *reduction* of the effective hole doping. Because this second channel involves the hybridization of the CuO_2 orbitals with only a small number of self-doping bands, it is expected to be more sensitive to δ_{api} than the first channel, which reflects global oxidation constraints and does not rely on a limited set of bands. Our calculations indicate that this second channel dominates in

Bi-2201/2212. As a consequence, increasing δ_{api} leads to a decrease of the effective hole-doping, in contrast to the behaviour observed in Hg-1201.

Conclusion We have presented material-specific predictions that clarify the role of the apical oxygen in the superconducting properties of cuprates. We answered the three central questions raised in the introduction. Variations of δ_{api} of the order of 10% lead to relative changes of m_{SC} of approximately 20%, and to relative variations of the superfluid density ranging from 30% (Bi-2212) to 40% (Bi-2201). By providing an absolute scale to these variations, we emphasize that these changes in m_{SC} are modest compared to those induced by other structural modifications, such as the transition from single-layer to bi-layer cuprates [question (i)]. This observation calls for caution when interpreting the proposed correlations between δ_{api} and T_c inferred from comparisons across different cuprate families [10, 14, 15, 18].

The quantitative agreement between our calculations and the STM measurements of Ref. [20] establishes apical oxygen displacement as the relevant microscopic mechanism underlying the periodic modulations of the superconducting order parameter in Bi-based cuprates [question (ii)]. At the same time, we provide compelling evidence that the variations of m_{SC} induced by δ_{api} are not governed by changes in the CTG. While the CTG remains a key energy scale for superconductivity in cuprates, it does not control the effect studied here. Instead, we demonstrate that variations of δ_{api} modify the effective hole-doping of the CuO_2 planes, which in turn drives the observed changes in m_{SC} [question (iii)]. Our analysis reveals that the relation between δ_{api} and effective doping is not universal across cuprate families. This highlights the importance of material-specific doping pathways for a quantitative understanding of superconductivity in cuprates.

Finally, one may envision leveraging the a -axis growth techniques already used for cuprates [52] to synthesize different compounds on a single sample. Such an approach would enable STM measurements similar to those of Ref. 20 to directly compare relative variations of m_{SC} across different cuprate materials, providing a stringent experimental test of our predictions.

Data availability The data and scripts used to generate the figures and the cif structure files have been deposited in the Open Science Framework repository [53].

Acknowledgments This work has been supported by the Natural Sciences and Engineering Research Council of Canada (NSERC) under grant ALLRP 588280-23 and by the Canada First Research Excellence Fund. The Canadian Foundation for Innovation, the Ministère de l'Économie, de l'Innovation et de l'Énergie (Québec), Calcul-Québec and the Digital Research Alliance of Canada provided part of the computational resources. This project was provided with computing HPC and storage resources by GENCI at TGCC, thanks to the grant 2024-A0170915694 on the supercomputer Joliot Curie's SKYLAKE and ROME partitions. This work of the Interdisciplinary Thematic Institute QMat, as part of the ITI 2021-2028 program of the University of Strasbourg, CNRS

and Inserm, was supported by IdEx Unistra (ANR 10 IDEX 0002), and by SFRI STRAT'US project (ANR 20 SFRI 0012) and EUR QMAT ANR-17-EURE-0024 under the framework of the French Investments for the Future Program. KH acknowledges support from NSF DMR-2233892 and a grant from the Simons Foundation (SFI-MPS-NFS- 00006741-06).

^a samuel.vadnais@utoronto.ca

^b benjamin.bacq-labreuil@ipcms.unistra.fr

- [1] G.-q. Zheng, Y. Kitaoka, K. Ishida, and K. Asayama, Local hole distribution in the CuO_2 plane of High- T_c Cu-oxides studied by Cu and Oxygen NQR/NMR, *Journal of the Physical Society of Japan* **64**, 2524 (1995).
- [2] J. Haase, O. P. Sushkov, P. Horsch, and G. V. M. Williams, Planar Cu and O hole densities in high- T_c cuprates determined with NMR, *Phys. Rev. B* **69**, 094504 (2004).
- [3] M. Jurkutat, D. Rybicki, O. P. Sushkov, G. V. M. Williams, A. Erb, and J. Haase, Distribution of electrons and holes in cuprate superconductors as determined from ^{17}O and ^{63}Cu nuclear magnetic resonance, *Phys. Rev. B* **90**, 140504 (2014).
- [4] D. Rybicki, M. Jurkutat, S. Reichardt, C. Kapusta, and J. Haase, Perspective on the phase diagram of cuprate high-temperature superconductors, *Nat Commun* **7**, 11413 (2016).
- [5] M. Jurkutat, C. Kattinger, S. Tsankov, R. Reznicek, A. Erb, and J. Haase, How pressure enhances the critical temperature of superconductivity in $\text{YBa}_2\text{Cu}_3\text{O}_{6+y}$, *Proceedings of the National Academy of Sciences* **120**, e2215458120 (2023).
- [6] L. Wang, G. He, Z. Yang, M. Garcia-Fernandez, A. Nag, K. Zhou, M. Minola, M. L. Tacon, B. Keimer, Y. Peng, and Y. Li, Paramagnons and high-temperature superconductivity in a model family of cuprates, *Nature Communications* **13**, 3163 (2022), publisher: Nature Publishing Group.
- [7] W. Ruan, C. Hu, J. Zhao, P. Cai, Y. Peng, C. Ye, R. Yu, X. Li, Z. Hao, C. Jin, X. Zhou, Z.-Y. Weng, and Y. Wang, Relationship between the parent charge transfer gap and maximum transition temperature in cuprates, *Science Bulletin* **61**, 1826 (2016).
- [8] Z. Wang, C. Zou, C. Lin, X. Luo, H. Yan, C. Yin, Y. Xu, X. Zhou, Y. Wang, and J. Zhu, Correlating the charge-transfer gap to the maximum transition temperature in $\text{Bi}_2\text{Sr}_2\text{Ca}_{n-1}\text{Cu}_n\text{O}_{2n+4+\delta}$, *Science* **381**, 227 (2023).
- [9] N. Kowalski, S. S. Dash, P. Sémond, D. Sénéchal, and A.-M. Tremblay, Oxygen hole content, charge-transfer gap, covalency, and cuprate superconductivity, *Proc. Natl. Acad. Sci. U.S.A.* **118**, e2106476118 (2021).
- [10] C. Weber, C. Yee, K. Haule, and G. Kotliar, Scaling of the transition temperature of hole-doped cuprate superconductors with the charge-transfer energy, *Europhysics Letters* **100**, 37001 (2012).
- [11] Z.-H. Cui, J. Yang, J. Tölle, H.-Z. Ye, S. Yuan, H. Zhai, G. Park, R. Kim, X. Zhang, L. Lin, T. C. Berkelbach, and G. K.-L. Chan, Ab initio quantum many-body description of superconducting trends in the cuprates, *Nature Communications* **16**, 1845 (2025).
- [12] B. Bacq-Labreuil, B. Lacasse, A.-M. Tremblay, D. Sénéchal, and K. Haule, Toward an ab initio theory of high-temperature superconductors: A study of multilayer cuprates, *Phys. Rev. X* **15**, 021071 (2025).
- [13] L. F. Feiner, M. Grilli, and C. Di Castro, Apical oxygen ions and the electronic structure of the high- T_c cuprates, *Phys. Rev. B* **45**, 10647 (1992).

[14] E. Pavarini, I. Dasgupta, T. Saha-Dasgupta, O. Jepsen, and O. K. Andersen, Band-structure trend in hole-doped cuprates and correlation with t_c max, *Phys. Rev. Lett.* **87**, 047003 (2001).

[15] P. R. C. Kent, T. Saha-Dasgupta, O. Jepsen, O. K. Andersen, A. Macridin, T. A. Maier, M. Jarrell, and T. C. Schulthess, Combined density functional and dynamical cluster quantum monte carlo calculations of the three-band hubbard model for hole-doped cuprate superconductors, *Phys. Rev. B* **78**, 035132 (2008).

[16] W.-G. Yin and W. Ku, Tuning the in-plane electron behavior in high- T_c cuprate superconductors via apical atoms: A first-principles wannier-states analysis, *Phys. Rev. B* **79**, 214512 (2009).

[17] C.-H. Yee and G. Kotliar, Tuning the charge-transfer energy in hole-doped cuprates, *Phys. Rev. B* **89**, 094517 (2014).

[18] Y. Peng, G. Dellea, M. Minola, M. Conn, A. Amorese, D. Di Castro, G. De Luca, K. Kummer, M. Salluzzo, X. Sun, *et al.*, Influence of apical oxygen on the extent of in-plane exchange interaction in cuprate superconductors, *Nature Physics* **13**, 1201 (2017).

[19] S. Acharya, C. Weber, E. Plekhanov, D. Pashov, A. Taraphder, and M. Van Schilfgaarde, Metal-insulator transition in copper oxides induced by apex displacements, *Phys. Rev. X* **8**, 021038 (2018).

[20] S. M. O'Mahony, W. Ren, W. Chen, Y. X. Chong, X. Liu, H. Eisaki, S. Uchida, M. H. Hamidian, and J. C. S. Davis, On the electron pairing mechanism of copper-oxide high temperature superconductivity, *Proc. Natl. Acad. Sci.* **119**, e2207449119 (2022), publisher: Proc. Natl. Acad. Sci.

[21] F. C. Zhang and T. M. Rice, Effective hamiltonian for the superconducting Cu oxides, *Phys. Rev. B* **37**, 3759 (1988).

[22] H. Sakakibara, H. Usui, K. Kuroki, R. Arita, and H. Aoki, Two-orbital model explains the higher transition temperature of the single-layer hg-cuprate superconductor compared to that of the La-cuprate superconductor, *Phys. Rev. Lett.* **105**, 057003 (2010).

[23] H. Sakakibara, H. Usui, K. Kuroki, R. Arita, and H. Aoki, Origin of the material dependence of t_c in the single-layered cuprates, *Phys. Rev. B* **85**, 064501 (2012).

[24] P. Hohenberg and W. Kohn, Inhomogeneous electron gas, *Phys. Rev.* **136**, B864 (1964).

[25] W. Kohn and L. J. Sham, Self-consistent equations including exchange and correlation effects, *Phys. Rev.* **140**, A1133 (1965).

[26] A. I. Lichtenstein and M. I. Katsnelson, Ab initio calculations of quasiparticle band structure in correlated systems: LDA++ approach, *Phys. Rev. B* **57**, 6884 (1998).

[27] A. I. Lichtenstein and M. I. Katsnelson, Antiferromagnetism and d-wave superconductivity in cuprates: A cluster dynamical mean-field theory, *Phys. Rev. B* **62**, R9283 (2000).

[28] G. Kotliar, S. Y. Savrasov, G. Pállsson, and G. Biroli, Cellular dynamical mean field approach to strongly correlated systems, *Phys. Rev. Lett.* **87**, 186401 (2001).

[29] G. Kotliar, S. Y. Savrasov, K. Haule, V. S. Oudovenko, O. Parcollet, and C. A. Marianetti, Electronic structure calculations with dynamical mean-field theory, *Rev. Mod. Phys.* **78**, 865 (2006).

[30] See Supplemental Material at [url xyz]. The following references are included in the Supplemental Material : [54–60].

[31] K. McElroy, J. Lee, J. A. Slezak, D.-H. Lee, H. Eisaki, S. Uchida, and J. C. Davis, Atomic-scale sources and mechanism of nanoscale electronic disorder in $\text{Bi}_2\text{Sr}_2\text{CaCu}_2\text{O}_{8+\delta}$, *Science* **309**, 1048 (2005).

[32] J. A. Slezak, J. Lee, M. Wang, K. McElroy, K. Fujita, B. M. Andersen, P. J. Hirschfeld, H. Eisaki, S. Uchida, and J. C. Davis, Imaging the impact on cuprate superconductivity of varying the interatomic distances within individual crystal unit cells, *Proc. Natl. Acad. Sci.* **105**, 3203 (2008).

[33] J. Hwang, Superconducting coherence length of hole-doped cuprates obtained from electron–boson spectral density function, *Scientific Reports* **11**, 11668 (2021).

[34] Model calculations based on an inhomogeneous Hubbard model with a modulation wavelength of 12-sites, close to experiment, lead to a correlation between hole-doping and $\epsilon_p - \epsilon_d$ modulation similar to what is found in our first-principles work, as can be seen in Fig. C.0.13 of Ref. [61]. In those calculations, $\epsilon_p - \epsilon_d$ is a phenomenological parameter.

[35] K. Haule, C.-H. Yee, and K. Kim, Dynamical mean-field theory within the full-potential methods: Electronic structure of CeIrIn_5 , CeCoIn_5 , and CeRhIn_5 , *Phys. Rev. B* **81**, 195107 (2010).

[36] K. Haule and G. L. Pascut, Forces for structural optimizations in correlated materials within a DFT+embedded DMFT functional approach, *Phys. Rev. B* **94**, 195146 (2016).

[37] K. Haule, Structural predictions for correlated electron materials using the functional dynamical mean field theory approach, *J. Phys. Soc. Jpn.* **87**, 041005 (2018).

[38] H. Lin, S. Sahrakorpi, R. S. Markiewicz, and A. Bansil, Raising Bi-O bands above the fermi energy level of hole-doped $\text{Bi}_2\text{Sr}_2\text{CaCu}_2\text{O}_{8+\delta}$ and other cuprate superconductors, *Phys. Rev. Lett.* **96**, 097001 (2006).

[39] J. Nokelainen, C. Lane, R. S. Markiewicz, B. Barbiellini, A. Pulkkinen, B. Singh, J. Sun, K. Pussi, and A. Bansil, Ab initio description of the $\text{Bi}_2\text{Sr}_2\text{CaCu}_2\text{O}_{8+\delta}$ electronic structure, *Phys. Rev. B* **101**, 214523 (2020).

[40] L. Bellaiche and D. Vanderbilt, The virtual crystal approximation revisited: Application to dielectric and piezoelectric properties of perovskites, *Phys. Rev. B* **61**, 7877 (2000).

[41] P. Blaha, K. Schwarz, F. Tran, R. Laskowski, G. K. H. Madsen, and L. D. Marks, Wien2k: An apw+lo program for calculating the properties of solids, *The Journal of Chemical Physics* **152**, 074101 (2020).

[42] T. N. Dionne, A. Foley, M. Rousseau, and D. Sénéchal, Pyqmc: An open-source python library for quantum cluster methods, *SciPost Physics Codebases* **10.21468/scipostphyscodeb.23** (2023).

[43] A. A. Mostofi, J. R. Yates, Y.-S. Lee, I. Souza, D. Vanderbilt, and N. Marzari, Wannier90: A tool for obtaining maximally-localised Wannier functions, *Comp. Phys. Comm.* **178**, 685 (2008).

[44] A. A. Mostofi, J. R. Yates, G. Pizzi, Y.-S. Lee, I. Souza, D. Vanderbilt, and N. Marzari, An updated version of Wannier90: A tool for obtaining maximally-localised Wannier functions, *Comp. Phys. Comm.* **185**, 2309 (2014).

[45] M. B. J. Meinders, H. Eskes, and G. A. Sawatzky, Spectral-weight transfer: Breakdown of low-energy-scale sum rules in correlated systems, *Phys. Rev. B* **48**, 3916 (1993).

[46] V. J. Emery, Theory of high- t_c superconductivity in oxides, *Phys. Rev. Lett.* **58**, 2794 (1987).

[47] C. Varma, S. Schmitt-Rink, and E. Abrahams, Charge transfer excitations and superconductivity in “ionic” metals, *Solid State Communications* **62**, 681 (1987).

[48] L. V. Pourovskii, B. Amadon, S. Biermann, and A. Georges, Self-consistency over the charge density in dynamical mean-field theory: A linear muffin-tin implementation and some physical implications, *Phys. Rev. B* **76**, 235101 (2007).

- [49] K. Haule, T. Birol, and G. Kotliar, Covalency in transition-metal oxides within all-electron dynamical mean-field theory, *Phys. Rev. B* **90**, 075136 (2014).
- [50] V. I. Anisimov, I. V. Solovyev, M. A. Korotin, M. T. Czyzyk, and G. A. Sawatzky, Density-functional theory and nio photoemission spectra, *Phys. Rev. B* **48**, 16929 (1993).
- [51] H. Eskes and J. H. Jefferson, Superexchange in the cuprates, *Phys. Rev. B* **48**, 9788 (1993).
- [52] Y. E. Suyolcu, J. Sun, B. H. Goodge, J. Park, J. Schubert, L. F. Kourkoutis, and D. G. Schlom, a-axis $\text{YBa}_2\text{Cu}_3\text{O}_{7-x}/\text{PrBa}_2\text{Cu}_3\text{O}_{7-x}/\text{YBa}_2\text{Cu}_3\text{O}_{7-x}$ trilayers with subnanometer rms roughness, *APL Materials* **9**, 021117 (2021).
- [53] <https://osf.io/62fsa>.
- [54] A. Levin, Y. I. Smolin, and Y. F. Shepelev, Causes of modulation and hole conductivity of the high- t_c superconductor $\text{Bi}_2\text{Sr}_2\text{CaCu}_2\text{O}_{8+x}$ according to x-ray single-crystal data, *Journal of Physics: Condensed Matter* **6**, 3539 (1994).
- [55] B. M. Andersen, P. J. Hirschfeld, and J. A. Slezak, Superconducting gap variations induced by structural supermodulation in $\text{Bi}_2\text{Sr}_2\text{CaCu}_2\text{O}_8$, *Phys. Rev. B* **76**, 020507 (2007).
- [56] Y. He, S. Graser, P. J. Hirschfeld, and H.-P. Cheng, Supermodulation in the atomic structure of the superconductor $\text{Bi}_2\text{Sr}_2\text{CaCu}_2\text{O}_{8+x}$ from ab initio calculations, *Phys. Rev. B* **77**, 220507 (2008).
- [57] C. Zou, Z. Hao, H. Li, X. Li, S. Ye, L. Yu, C. Lin, and Y. Wang, Effect of structural supermodulation on superconductivity in trilayer cuprate $\text{Bi}_2\text{Sr}_2\text{Ca}_2\text{Cu}_3\text{O}_{10+\delta}$, *Phys. Rev. Lett.* **124**, 047003 (2020).
- [58] Z. Jin and S. Ismail-Beigi, First-principles prediction of structural distortions in the cuprates and their impact on the electronic structure, *Phys. Rev. X* **14**, 041053 (2024).
- [59] K. Haule, Quantum monte carlo impurity solver for cluster dynamical mean-field theory and electronic structure calculations with adjustable cluster base, *Phys. Rev. B* **75**, 155113 (2007).
- [60] K. Haule, Exact Double Counting in combining the dynamical mean field theory and the density functional theory, *Phys. Rev. Lett.* **115**, 196403 (2015).
- [61] F. Rotella, *Theoretical methods for the role of correlations on high- T_c superconductivity*, Theses, Université Paris-Saclay (2024).
- [62] J. Hubbard, Electron correlations in narrow energy bands, *Proceedings of the Royal Society of London. A. Mathematical and Physical Sciences* **276**, 238 (1963).
- [63] M. C. Gutzwiller, Effect of correlation on the ferromagnetism of transition metals, *Phys. Rev. Lett.* **10**, 159 (1963).
- [64] J. Kanamori, Electron correlation and ferromagnetism of transition metals, *Progress of Theoretical Physics* **30**, 275 (1963).
- [65] S. S. Dash and D. Sénéchal, Pseudogap transition within the superconducting phase in the three-band hubbard model, *Phys. Rev. B* **100**, 214509 (2019).

END MATTER

A simplified view of the variations in effective hole-doping

In the main text, we interpreted the variations of occupation in terms of charge transfer between different planes and electronic degrees of freedom in the crystal structure. While physically transparent, this picture is not easily translated into the language of low-energy effective models, which is commonly used in the cuprate literature. The purpose of this section is therefore to provide an alternative, simplified description of these effects within the framework of a single-band Hubbard model [62–64].

Our starting point is the DFT-only calculations performed for each apical oxygen distance in Bi-2201/2212. We parameterize a single-band Hubbard model using Wannier orbitals: we keep the in-plane hopping terms t , t' , t'' , up to the next-next-nearest neighbor, and for Bi-2212 we include the inter-plane hopping term t_{\perp} (001), t'_{\perp} (111) and t''_{\perp} (201/021). The corresponding Hamiltonians read:

$$H_{2201}(\delta_{\text{api}}) = - \sum_{\langle i,j \rangle, \sigma} t_{ij}(\delta_{\text{api}}) [c_{i,\sigma}^{\dagger} c_{j,\sigma} + \text{h.c.}] \quad (1)$$

$$+ U \sum_i n_{i,\uparrow} n_{i,\downarrow} + [\epsilon(\delta_{\text{api}}) - \mu] \sum_{i,\sigma} n_{i,\sigma},$$

$$H_{2212}(\delta_{\text{api}}) = - \sum_{\langle i,j \rangle, \sigma, \alpha} t_{ij}(\delta_{\text{api}}) [c_{i,\sigma}^{\alpha\dagger} c_{j,\sigma}^{\alpha} + \text{h.c.}] \quad (2)$$

$$- \sum_{\langle i,j \rangle, \sigma, \alpha} t_{\perp,ij}(\delta_{\text{api}}) [c_{i,\sigma}^{\alpha\dagger} c_{j,\sigma}^{\bar{\alpha}} + \text{h.c.}]$$

$$+ U \sum_i n_{i,\uparrow} n_{i,\downarrow} + [\epsilon(\delta_{\text{api}}) - \mu] \sum_{i,\sigma} n_{i,\sigma},$$

where $t_{ij} = t$, t' or t'' , and $t_{\perp,ij} = t_{\perp}$, t'_{\perp} or t''_{\perp} , α and $\bar{\alpha}$ designate the CuO_2 plane in the bi-layer model, ϵ is the on-site energy, and μ the chemical potential. All model parameters are taken to depend on δ_{api} , except for the chemical potential. We compute the non-interacting ($U = 0$) density of states (DOS) for the effective $H_{2201/2212}$ models at each value of δ_{api} . The same chemical potential μ is used for all δ_{api} , reflecting the fact that the remainder of the crystal acts as an effective reservoir that fixes the chemical potential of the CuO_2 planes. We choose μ such that the $\delta_{\text{api}} = 2.30 \text{ \AA}$ models are effectively at 20% hole-doping, i.e., in a representative doping range compared to our calculation (our analysis is not sensitive to this specific choice of μ).

The resulting DOS are shown in Fig. 5(a1,a2). For Bi-2201, the particle-hole asymmetry of the DOS increases with δ_{api} . As a result, the van Hove singularity shifts towards the occupied part of the spectrum, leading to an increase in the occupation with increasing δ_{api} . This is not necessarily related to a change of on-site occupation $\epsilon(\delta_{\text{api}})$, but rather to (i) the common chemical potential μ for all δ_{api} , and (ii) the increase of both t'/t and t''/t with δ_{api} (we provide the resulting parameters in the SM [30]). Hence, in terms of an effective model, the

variations in occupation should not be seen as caused by variations of on-site energies, but rather by variations of particle-hole asymmetry of the underlying non-interacting DOS.

In the case of Bi-2212, the asymmetry of the non-interacting DOS is also at play, but the mechanism is slightly different. We find that the in-plane hoppings are almost independent of δ_{api} , in contrast with the out-of-plane hoppings, which decrease with increasing δ_{api} (the distance between the two CuO_2 planes increases). As such, the coupling between the two planes decreases, which leads to a lower splitting between the bonding and anti-bonding bands, as can be seen in Fig. 5(a2). Similarly to Bi-2201, the occupation rises with increasing δ_{api} .

These results are summarized in Fig. 5(c). The increased occupation in the non-interacting effective models for Bi-2201/2212 mimics accurately our DFT+CDMFT results. The variations are quantitatively larger than in the realistic calculations, probably because we ignored the on-site interaction U .

Witnessing the change in effective hole-doping in the Fermi surface and the spectral function

The variations in effective doping of the CuO_2 planes are manifest in the spectral properties. In Fig. 6(a) we show the periodized momentum-resolved spectral function of Bi-2201 along the $\Gamma(0,0) - X(\pi,0) - M(\pi,\pi) - \Gamma$ path, for the two extreme apical distances $\delta_{\text{api}} = 2.30 \text{ \AA}$ and $\delta_{\text{api}} = 2.53 \text{ \AA}$. As expected from the three-band Wannierization detailed in the main text, the two spectral functions are very similar. One notices that the occupied spectrum of the smallest apical distance is slightly shifted closer to the Fermi level, consistent with its higher hole-doping. The main signature of the change in doping is the pseudogap around the anti-nodal (X) region. As shown in Fig. 6(b), the pseudogap is smaller for $\delta_{\text{api}} = 2.30 \text{ \AA}$, since the effective hole doping is larger. This finally translates into the Fermi surface shown in Fig. 6(c). The arcs are much more extended for $\delta_{\text{api}} = 2.30 \text{ \AA}$, which again clearly demonstrates that the smallest apical distance corresponds to the largest hole doping.

Varying U

We need to check that our results are robust against variations of the on-site interaction U . Indeed, U is the *only* free parameter in our approach, and it is known to have a substantial effect on the superconducting order parameter m_{SC} .

We therefore compute m_{SC} with respect to δ_{api} in Bi-2212 using a range of on-site interactions $U = 8, 9, 10, 11 \text{ eV}$. As shown in Fig. 7, the absolute value of m_{SC} is, as expected, inversely correlated with U . However, the relative variations of the superfluid density $|m_{\text{SC}}|^2 / \overline{|m_{\text{SC}}|^2}$ for $U = 8 - 10 \text{ eV}$ remain in quantitative agreement with the STM measurements of Ref. [20]. Interestingly, a deviation is observed for

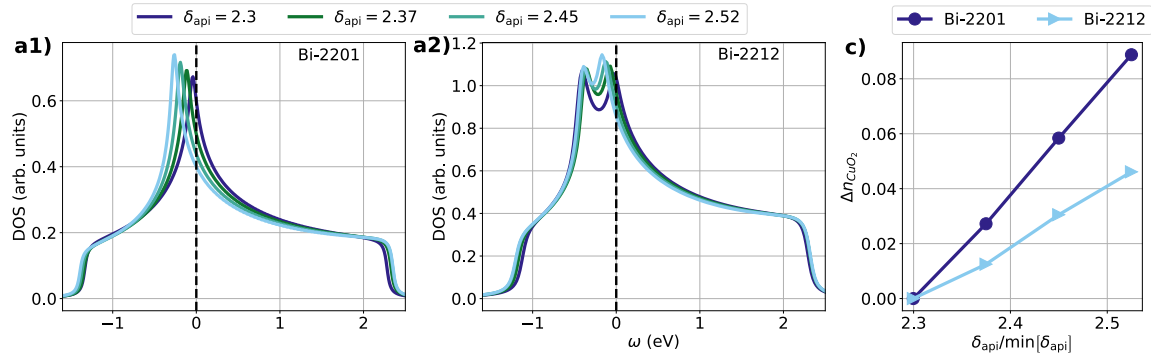


FIG. 5. Non-interacting DOS of the low-energy effective model of (a1) Bi-2201 and (b1) Bi-2212 for all values of δ_{api} . (b) Variations of occupation Δn_{CuO_2} estimated from the non-interacting effective models.

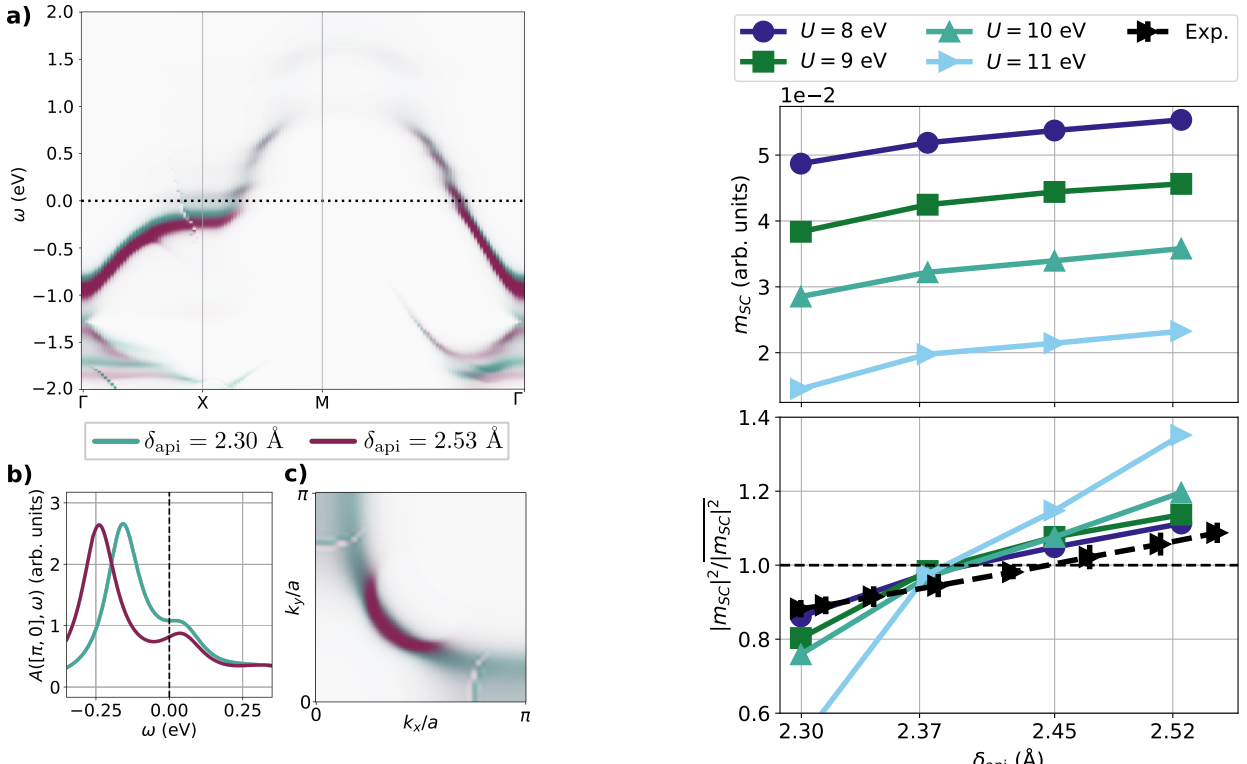


FIG. 6. (a) Periodized momentum-resolved spectral function projected on the Cu- $d_{x^2-y^2}$ orbital, in the normal state of Bi-2201 for the two extreme values of δ_{api} . (b) Spectral functions at the antinodal X ($\pi, 0$) point. (c) Corresponding super-imposed Fermi surfaces for the two extreme values of δ_{api} .

$U = 11$ eV. This is consistent with the fact that self-doping effectively brings the CuO_2 into the overdoped regime. In this regime, studies of the covalent Emery model show that increasing U pushes the frontier of the superconducting dome to lower critical doping and increases the steepness of the dome [9, 65]. At $U = 11$ eV, the system has reached the end of the overdoped side of the dome, and thus the relative variations increase more drastically.

Hence, this additional analysis not only demonstrates the robustness of our results but also reinforces our interpretation

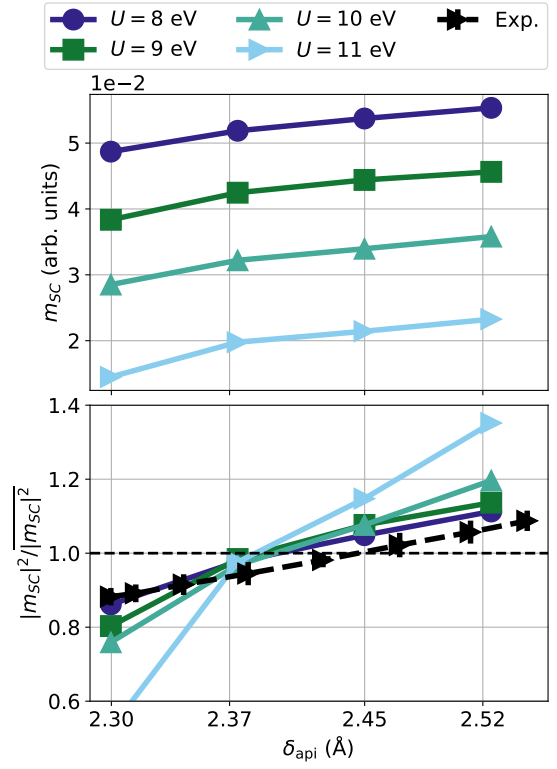


FIG. 7. Computed superconducting order parameter m_{SC} vs δ_{api} for Bi-2212 using different values of U (top). Note the y -axis scaling. Relative variations of the computed and measured superfluid density $|m_{\text{SC}}|^2 / \overline{|m_{\text{SC}}|^2}$ vs δ_{api} (bottom). The experimental data are digitized from Ref. 20.

based on variations of the effective hole doping.

SUPPLEMENTAL MATERIAL FOR "THE ROLE OF THE APICAL OXYGEN IN CUPRATE HIGH-TEMPERATURE SUPERCONDUCTORS"

Computational details

Structure optimisation – The study of Bi-based cuprates in their full structural complexity within our DFT+CDMFT framework poses a considerable challenge that we cannot overcome. The primary difficulty stems from the long-range supermodulation of the crystal structure [20, 54–58], which necessitates an enlarged effective unit cell containing several hundred atoms. Since our main goal is to isolate the effect of the apical distance δ_{api} , we decompose the $\text{Bi}_2\text{Sr}_2\text{CuO}_{6+\delta}$ (Bi-2201) supercell into a series of homogeneous tetragonal systems in which δ_{api} is varied following values expected from experiments [20]. The resulting structures are subsequently relaxed within DFT + single-site DMFT while maintaining δ_{api} constant, using the implementation of the eDMFT package [35–37].

For the structure optimisation of Bi-2201, the correlated subspace contains both $\text{Cu-}d_{x^2-y^2}$ and d_{z^2} orbitals. We use the hybridization-expansion continuous time quantum Monte Carlo solver of Ref. 59 with $U = 12$ eV and $J_{\text{Hund}} = 1$ eV at the inverse temperature $\beta = 50$ eV $^{-1}$, and the exact double-counting scheme of Ref. 60 with a mixture of Yukawa and dielectric screening

$$V_{\text{DMFT}}(\mathbf{r}, \mathbf{r}') = \frac{e^{-\lambda|\mathbf{r}-\mathbf{r}'|}}{\epsilon|\mathbf{r}-\mathbf{r}'|}, \quad (3)$$

where λ and ϵ are constant that can be uniquely determined from the value of U and J_{Hund} . The radius of muffin-tins (RMT) was kept constant for all different homogeneous systems, with their values being given by the most constraining δ_{api} value. During this step, a momentum grid of size 12x12x12 is used. Force convergence is reached when forces between all atoms (except apical oxygen, which is kept fixed) are smaller than 2.0 mRy/Bohr.

This structure optimisation step is repeated with various values of unit cell parameters a and c to find the most energetically favourable combination, using splines to interpolate the equilibrium values. The results of this optimisation are shown in Table I, where a is found to be constant across all values of δ_{api} considered, and c varies following δ_{api} modulations. With the unit-cell parameters optimised, a final unit-cell is constructed for each δ_{api} value, and atomic positions are relaxed one last time.

We assumed a similar dependence of a and c with respect to variations of δ_{api} for the two other compounds – $\text{Bi}_2\text{Sr}_2\text{CaCu}_2\text{O}_{8+x}$ (Bi-2212) and $\text{HgBa}_2\text{CuO}_{4+\delta}$ (Hg-1201). The experimental unit cell parameters of Bi-2212 are used for the average value of δ_{api} , and c is adjusted following the δ_{api} vs c relation of Bi-2201. The same is done for Hg-1201, but in this case the equilibrium unit-cell corresponds to the largest δ_{api} .

TABLE I. Unit-cell parameter of the optimised I4/mmm homogeneous Bi-2201 systems

δ (Å)	a (Å)	c (Å)
2.299		23.637
2.374		24.130
2.449	3.762	24.376
2.525		24.868

DFT+CDMFT calculations – To compute the superconducting order parameter m_{SC} , we then resort to DFT+CDMFT calculations. We construct 2×2 supercells from the optimised structures. They can be found in the Open Science Framework repository as *.cif files [53]. To keep the number of atoms tractable in Bi-2201/2212, we first transform the structure from I4/mmm to P4/mmm before constructing the supercell. We showed in a previous work that such structure simplification in cuprates leaves the low-energy subspace unchanged [12]. For each structure, we fix the RMT value for all apical distances and take a 2×2 plaquette of $\text{Cu-}d_{x^2-y^2}$ orbitals as the correlated subspace. We set $U = 9$ eV and $J_{\text{Hund}} = 1$ eV. The impurity problem is solved with exact diagonalization [42] using a fictitious inverse temperature $\beta = 50$ eV $^{-1}$ for the definition of the Matsubara frequencies. We use the exact DC scheme as described above. Note that a smaller U value is used for cluster calculations compared to our previous study [12]. This is because the DC correction now includes the angle-dependence of the $\text{Cu-}d_{x^2-y^2}$ orbital, which was ignored previously, thereby changing the estimation. As discussed in the End Matter, we show that our results are robust against large variations of U . We use a $12 \times 12 \times 8$ k-grid for the DFT+CDMFT convergence in the normal state. The virtual crystal approximation (VCA) [40] is applied to the Hg atoms in Hg-1201.

To compute the order parameter m_{SC} , we use the same post-processing method as described in Ref. 12, with a $16 \times 16 \times 4$ k-grid. For Bi-2212, we include proximity effects between the two adjacent CuO_2 planes. The order parameter m_{SC} is obtained

from the lattice average of the pair operator \hat{D}_{SC} :

$$\begin{aligned}\hat{D}_{\text{SC}} &= \frac{1}{2} \left[\sum_{\langle ij \rangle_x} \left(d_{i\uparrow}^\dagger d_{j\downarrow}^\dagger - d_{i\downarrow}^\dagger d_{j\uparrow}^\dagger \right) - \sum_{\langle ij \rangle_y} \left(d_{i\uparrow}^\dagger d_{j\downarrow}^\dagger - d_{i\downarrow}^\dagger d_{j\uparrow}^\dagger \right) + \text{H.c.} \right], \\ m_{\text{SC}} &= \frac{1}{\beta L N_k} \text{Tr}_{\omega_n, \mathbf{k}} \left(G(\mathbf{k}, i\omega_n) \cdot \hat{D}_{\text{SC}}(\mathbf{k}) \right),\end{aligned}\quad (4)$$

where $\text{Tr}_{\omega_n, \mathbf{k}}(\cdot)$ means the trace over Matsubara frequencies $i\omega_n$, superlattice momentum \mathbf{k} and cluster indices, L the number of cluster orbitals and N_k the number of k -points.

A detailed presentation of the method is provided in Ref. 12.

Effective Emery–Varma–Schmitt–Rink–Abrahams Hamiltonian

The Emery–Varma–Schmitt–Rink–Abrahams three-band model [46, 47] reads

$$\begin{aligned}\mathcal{H} &= \sum_{\mathbf{k}, \sigma} \Psi_{\mathbf{k}, \sigma}^\dagger \mathbf{h}_0(\mathbf{k}) \Psi_{\mathbf{k}, \sigma} + U \sum_i n_{i\uparrow}^d n_{i\downarrow}^d, \\ \mathbf{h}_0(\mathbf{k}) &= \begin{pmatrix} -\mu & t_{pd}(1 - e^{-ik_x}) & t_{pd}(1 - e^{-ik_y}) \\ t_{pd}(1 - e^{ik_x}) & \Delta_p - \mu & \frac{t_{pp}(1 - e^{ik_x})}{(1 - e^{-ik_y})} \\ t_{pd}(1 - e^{ik_y}) & \frac{t_{pp}(1 - e^{-ik_x})}{(1 - e^{ik_y})} & \Delta_p - \mu \end{pmatrix},\end{aligned}\quad (5)$$

where the spinor $\Psi_{\mathbf{k}, \sigma}^\dagger = (d_{\mathbf{k}, \sigma}^\dagger, p_{\mathbf{k}, \sigma}^{x\dagger}, p_{\mathbf{k}, \sigma}^{y\dagger})$ contains the creation operators for the Cu- $d_{x^2-y^2}$ and O- $p_{x/y}$ orbitals at wave vector \mathbf{k} and spin σ . Setting the Cu- $d_{x^2-y^2}$ on-site energy to zero, Δ_p denotes the on-site energy of the O- $p_{x/y}$ orbitals, μ is the chemical potential, and t_{pd} (t_{pp}) are the Cu–O (nearest O–O) hopping amplitudes.

Hopping parameters for the effective single-band models

In the End Matter, we provided a simplified view of the variations in effective hole-doping in Bi-2201 and Bi-2212 using single-band Hubbard models obtained with Wannier90 [43, 44]. We present in Table II and Table III the parameters for Bi-2201 and Bi-2212, respectively. The on-site energy ϵ is rigidly shifted for all apical distances such that the lowest apical distance reaches an effective hole-doping of 20%.

δ_{api} (Å)	t (eV)	t'/t	t''/t	ϵ/t
2.299	0.452	-0.143	0.083	-0.808
2.374	0.459	-0.166	0.102	-0.817
2.449	0.465	-0.184	0.117	-0.786
2.525	0.468	-0.200	0.128	-0.737

TABLE II. Hopping parameters t , t' , t'' and on-site energy ϵ of Bi-2201 single-band Hubbard model.

δ_{api} (Å)	t (eV)	t'/t	t''/t	t_{\perp}/t	t'_{\perp}/t	t''_{\perp}/t	ϵ/t
2.299	0.427	-0.246	0.149	0.166	-0.061	0.029	-0.986
2.374	0.436	-0.234	0.148	0.111	-0.045	0.020	-0.967
2.449	0.440	-0.238	0.153	0.093	-0.045	0.015	-0.933
2.525	0.441	-0.247	0.159	0.085	-0.043	0.014	-0.912

TABLE III. Hopping parameters t , t' , t'' , t_{\perp} , t'_{\perp} , t''_{\perp} and on-site energy ϵ of Bi-2212 single-band bi-layer Hubbard model. The inter-layer hopping t_{\perp} correspond to hopping in the $(0, 0, \pm 1)$ direction, t'_{\perp} to $(\pm 1, \pm 1, \pm 1)/(\pm 1, \mp 1, \pm 1)$ and t''_{\perp} to $(\pm 2, 0, \pm 1)/(0, \pm 2, \pm 1)$.

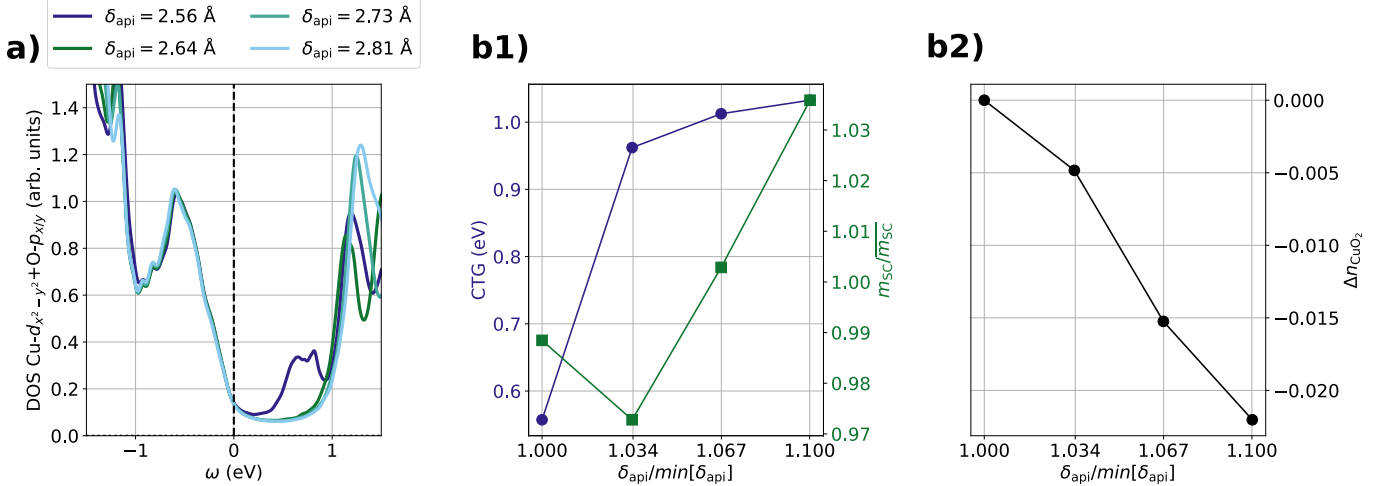


FIG. 8. (a) DFT+CDMFT DOS projected on the Cu- $d_{x^2-y^2}$ and O- $p_{x/y}$ orbitals of undoped Hg-1201. (b1) Charge transfer gap (dark blue) extracted from the projected density of states for undoped Hg-1201 with respect to the apical distance. Relative variations of m_{SC} (green) for underdoped Hg-1201 vs. δ_{api} . (b2) Variations of the CuO_2 plane occupation vs. the apical distance in underdoped Hg-1201, using the lowest apical distance as reference.

Hg-1201: investigating further the role of the CTG.

The Hg-based compound enables further study of the link between the CTG and the apical distance δ_{api} . Indeed, in undoped Hg-1201, the CuO_2 planes remain insulating with a well-defined CTG [12]. We thus performed calculations for undoped Hg-1201 for all apical distances. The CTG is unambiguously visible in the density of states (DOS) projected on the Cu- $d_{x^2-y^2}$ and O- $p_{x/y}$ orbitals, as shown in Fig. 8(a). As anticipated in the case of Bi-based cuprates, the CTG is *correlated* with δ_{api} .

The evolution of the CTG, of m_{SC} and of the CuO_2 plane occupation n_{CuO_2} vs δ_{api} are summarized in Fig. 8(b1,b2). We recall that the CTG is obtained from undoped Hg-1201, while m_{SC} and Δn_{CuO_2} are extracted from calculations in the underdoped regime (using the VCA). Overall, both m_{SC} and the CTG increase with δ_{api} , while Δn_{CuO_2} decreases. It appears clearly that the CTG *competes* with the variations of hole doping in Hg-1201: for $\delta_{\text{api}}/\min[\delta_{\text{api}}] > 1.034$ the small increase of CTG (detrimental to m_{SC}) is overwhelmed by the rise of the effective hole doping (favourable to m_{SC} in the underdoped regime). This competition is confirmed by the first decrease of m_{SC} between the two lowest δ_{api} : the small rise in hole doping is overwhelmed by the drastic increase of the CTG.

This additional analysis of Hg-1201 strikingly confirms the main message of this work: while the CTG is pivotal to superconductivity in cuprates [9, 10, 12], it cannot explain the relation between δ_{api} and m_{SC} .